

High Performance OTFTs Fabricated Using a Calamitic Liquid Crystalline Material of 2-(4-Dodecyl phenyl)[1]benzothieno[3,2-*b*][1]benzothiophene

Yaowu He, Melda Sezen, Dongwei Zhang, Aiyuan Li, Lijia Yan, Hongtao Yu, Chao He, Osamu Goto,* Yueh-Lin Loo,* and Hong Meng*

An air-stable calamitic liquid crystalline material, 2-(4-dodecyl phenyl)[1]benzothieno[3,2-*b*]benzothiophene (C12-Ph-BTBT), is designed with a highly ordered smectic X (SmX) (X = K or H) phase demonstrating high charge-carrier mobility and thermal stability in thin-film transistors. Organic thin-film transistors show mobilities as high as $8.7 \text{ cm}^2 \text{ V}^{-1} \text{ s}^{-1}$ when the C12-Ph-BTBT thin film is annealed at its SmX phase before the electrode deposition. Structural characterization reveals that the as-deposited C12-Ph-BTBT thin films adopt a unilamellar structure. On the other hand, after polycrystalline thin films of C12-Ph-BTBT exhibit bilayer structure after annealing at the temperature of the SmX and the smectic E phases. The highest charge-carrier mobility is observed when the C12-Ph-BTBT thin films are annealed at the SmX phase before the electrode deposition. The results give insight into the understanding of the nature of the mesophase behavior of liquid-crystalline semiconductors and can aid the rational design of self-organizing molecular semiconductors.

materials have been considered as promising candidates for OTFTs^[11–17] because these materials can form well-ordered polycrystalline thin films with large aligned domains as-deposited or after thermal annealing to promote structuring in liquid-crystalline phases.^[18–20] Self-assembly with high degrees of intermolecular order facilitates charge transport in organic semiconductors. Recent work has demonstrated the use of a new rod-like liquid-crystalline organic semiconductor, 2-decyl-7-phenyl-[1]benzothieno[3,2-*b*][1]benzothiophene (Ph-BTBT-10), with a highly ordered smectic E (SmE) mesophase for OTFT applications.^[17] Fabricated polycrystalline OTFTs showed mobilities as high as $13.9 \text{ cm}^2 \text{ V}^{-1} \text{ s}^{-1}$ with good thin-film uniformity and high thermal durability.^[17] Despite its high performance in

1. Introduction

Organic thin-film transistors (OTFTs) have been extensively investigated because they can be fabricated with low-temperature and low-cost processes, providing potential utility in lightweight, nonbreakable, and flexible electronics.^[1–6] In order to realize next-generation large-area and high-definition flexible and/or rollable displays, we need pixel-addressing OTFTs with high mobility for backplanes. Several years ago, it was thought that only single-crystal devices are capable of meeting the high mobility requirements of such applications.^[7–10] However, it remains challenging to control the thickness and the crystal orientation of the single crystals. Recently, liquid-crystalline

OTFTs, Ph-BTBT-10 exhibits a phase transition from its crystalline phase to its SmE phase at around $140 \text{ }^\circ\text{C}$; above which the mobility of Ph-BTBT-10-based OTFTs decreases drastically. However, the thermal stability is indispensable to the liquid crystals in OTFT applications. Meanwhile, a simple synthetic route for large-scale production has to be also considered to maintain the low-cost aspects of OTFTs.

In this paper, we focus on the investigation of an air-stable, rodlike, liquid-crystalline molecular semiconductor, 2-(4-dodecyl phenyl)[1]benzothieno[3,2-*b*]benzothiophene (C12-Ph-BTBT). Unlike Ph-BTBT-10, which only exhibits one ordered liquid-crystalline phase (SmE phase), C12-Ph-BTBT shows three liquid-crystalline phases, including a more ordered smectic X (SmX) phase (X = K or H). Interestingly, structural characterization by X-ray diffraction (XRD), grazing-incidence X-ray diffraction (GIXD), and atomic force microscopy (AFM) reveals that while the as-deposited C12-Ph-BTBT thin films exhibit a unilamellar structure, they transition to a bilayer polycrystalline structure after annealing at the temperatures of the SmX and the SmE phases. Devices with the highest mobility ($8.7 \text{ cm}^2 \text{ V}^{-1} \text{ s}^{-1}$) are obtained when C12-Ph-BTBT thin film is annealed at its SmX phase. Though this rodlike liquid-crystalline family of C12-Ph-BTBT has been patented,^[21] its charge transport characteristics in the different smectic phases, especially in the SmX phase, has not been systematically investigated.

Here, we elucidate the liquid-crystalline behavior of C12-Ph-BTBT and its effects on the performance of C12-Ph-BTBT-based

Dr. Y. He, Dr. D. Zhang, Dr. A. Li, L. Yan, Dr. H. Yu,
Dr. C. He, Prof. O. Goto, Prof. H. Meng
School of Advanced Materials
Peking University Shenzhen Graduate School
Peking University
Shenzhen 518055, China
E-mail: ogoto@pkusz.edu.cn; menghong@pkusz.edu.cn



M. Sezen, Prof. Y.-L. Loo
Department of Chemical and Biological Engineering
Princeton University
Princeton, NJ 08544, USA
E-mail: lloo@princeton.edu

DOI: 10.1002/aelm.201600179

OTFTs. We fabricated OTFTs by two different procedures. In one case, we thermally annealed evaporated thin films of C12-PH-BTBT first, followed by the deposition of the source/drain (S/D) electrodes to fabricate top-contact OTFTs. In the second case, we fabricated the OTFTs first, and then thermally annealed the device stack subsequently. The highest mobility is achieved when devices with C12-Ph-BTBT thin films are annealed to reach the SmX phase before depositing contacts. We observe the presence of highly ordered crystalline structures with large (up to 20 μm diameter) domains by polarized optical microscopy (POM) under these annealing conditions.

2. Results and Discussion

Figure 1 shows the liquid-crystalline properties of C12-Ph-BTBT. Figure 1a describes the chemical structure of C12-Ph-BTBT, Figure 1b shows the differential scanning calorimetry (DSC) traces, and Figure 1c shows the powder XRD traces at various temperatures during cooling. Figure 1d–g shows polarized optical microscope images of C12-Ph-BTBT thin films at 50, 100, 170, and 200 $^{\circ}\text{C}$ acquired during cooling. As seen in Figure 1b, C12-Ph-BTBT has three characteristic liquid-crystalline phases. The high-temperature liquid-crystalline phase that exists between 209.9 and 172.3 $^{\circ}\text{C}$ shows a typical fan-like texture without disclination lines as seen in the

polarized optical micrograph in Figure 1g, and only one peak is observed at $2\theta = 5.6^{\circ}$ in the XRD pattern obtained at 180 $^{\circ}\text{C}$ in Figure 1c. These observations are characteristics of a liquid-crystalline smectic A (SmA) phase. While the intermediate liquid-crystalline phase between 172.3 and 135.2 $^{\circ}\text{C}$ also shows fan-like texture, disclination lines can be clearly seen in the optical micrograph in Figure 1f. In addition to the peak at 5.6° , peaks at 4.7° , 6.9° , and 14.1° (corresponding to d-spacings of 18.9, 12.7, and 6.3 \AA) start appearing in the XRD pattern obtained at 150 $^{\circ}\text{C}$ in Figure 1c. We identified this intermediate phase as a SmE phase (from SmA to SmE, $\Delta H = 14.79 \text{ J g}^{-1}$). A larger enthalpy ($\Delta H = 45.62 \text{ J g}^{-1}$) is observed at 135.2 $^{\circ}\text{C}$. It represents a transition from SmE to a higher ordered phase. Moreover, a small enthalpy ($\Delta H = 7.35 \text{ J g}^{-1}$) has been detected at 65 $^{\circ}\text{C}$. It indicates the transition from a more order phase to a crystal. According to a decrease in entropy of the liquid-crystal phase, the phase between 65 and 135.2 $^{\circ}\text{C}$ should be the SmK or H phase.^[22] Given that we are not able to definitively identify this phase, however, we refer to it as an SmX phase. This SmX phase does not exhibit fan-like texture (Figure 1e).

Figure 2 summarizes the morphology of C12-Ph-BTBT polycrystalline thin films. Figure 2a–c shows polarized microscope images of the as-deposited films, and the films that are annealed at 140 $^{\circ}\text{C}$ for 10 min, and at 170 $^{\circ}\text{C}$ for 5 min, respectively. Figure 2d–f shows the corresponding AFM images of these samples, and the cross-section profiles extracted from these AFM

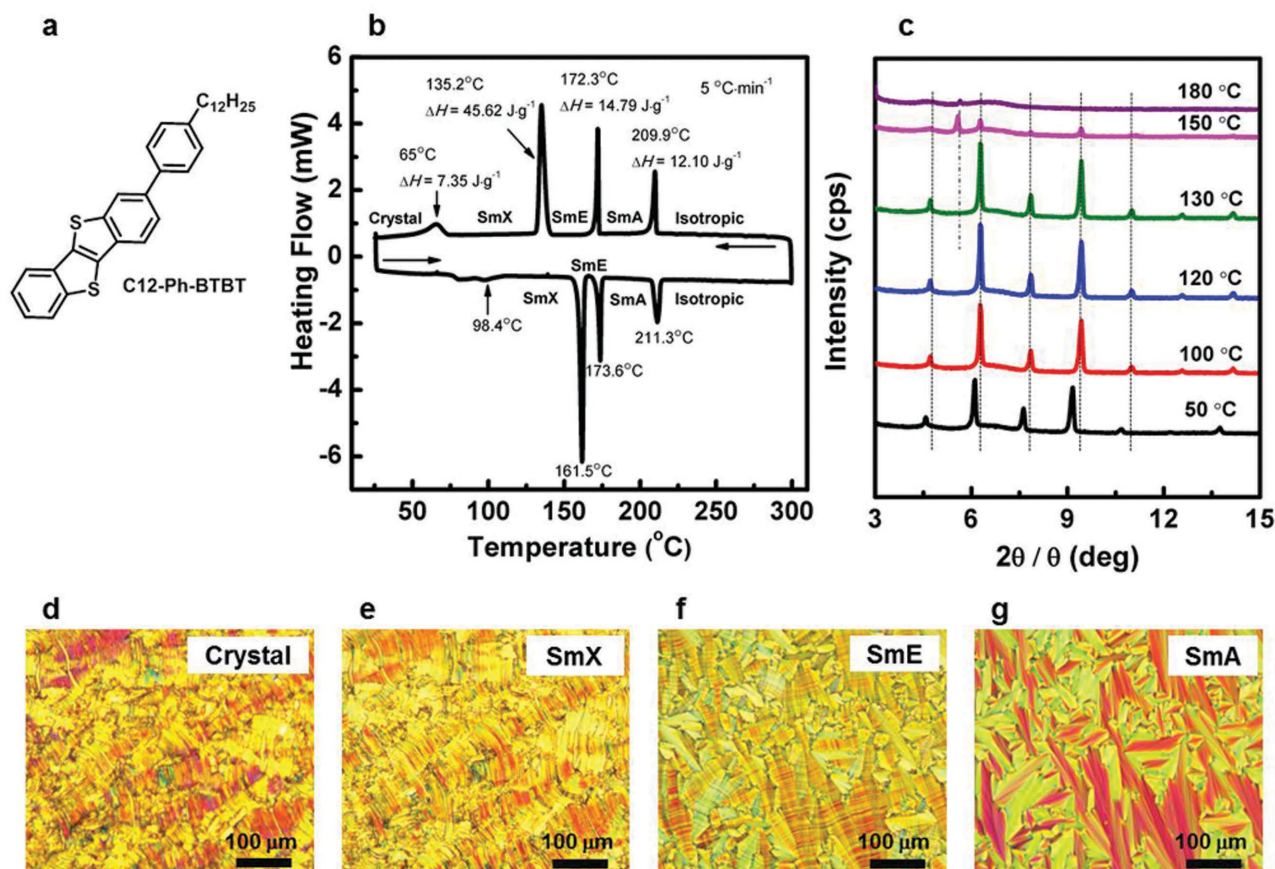


Figure 1. Results of liquid crystal characteristics of C12-Ph-BTBT powder: a) chemical structure, b) DSC curve, c) XRD patterns at various temperatures during cooling. Polarized optical microscope images of d) crystal (50 $^{\circ}\text{C}$), e) SmX (100 $^{\circ}\text{C}$), f) SmE (170 $^{\circ}\text{C}$), and g) SmA (200 $^{\circ}\text{C}$) phases.

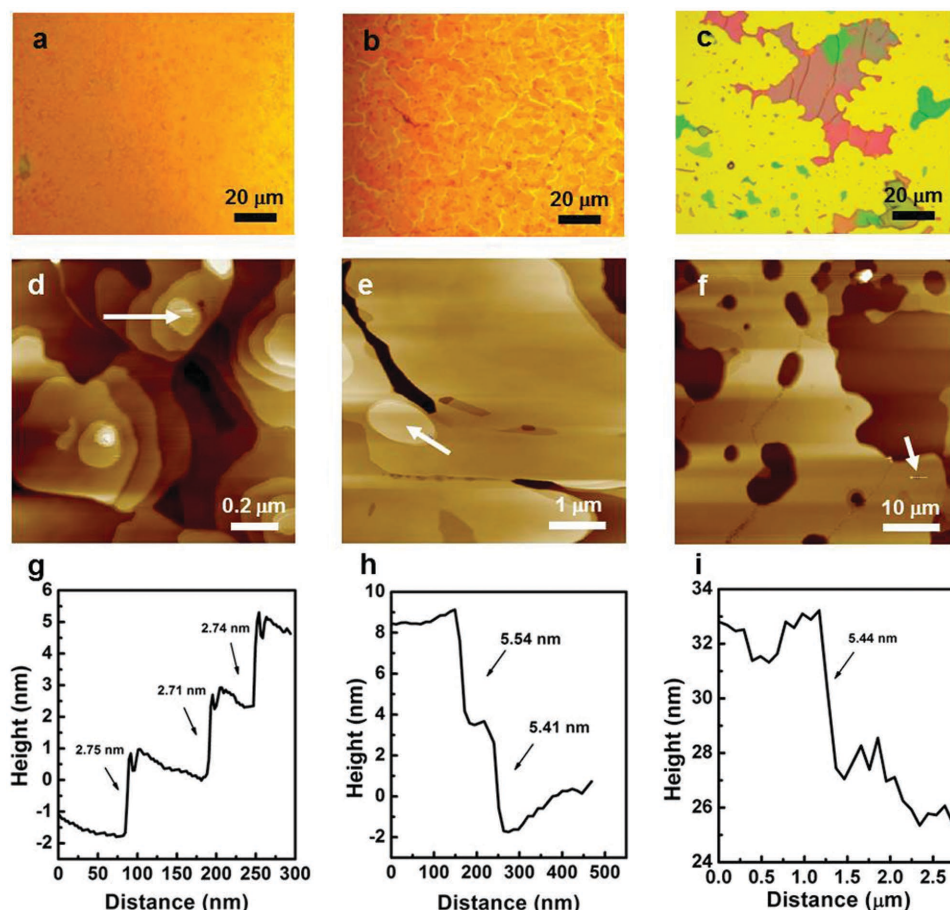


Figure 2. Polarized microscope images of polycrystalline C12-Ph-BTBT thin films a) as-deposited, b) annealed at 140 °C for 10 min, and c) annealed at 170 °C for 5 min. d–f) AFM images, and g–i) cross-sectional profiles of the samples in (a), (b), and (c), respectively. Scanning position and direction are also indicated in (d), (e), and (f).

images are given in Figure 2g–i (the scanning positions and directions are labeled with white arrows on the micrographs). The as-deposited C12-Ph-BTBT thin film in Figure 2a is featureless; AFM reveals the presence of islands with a step height of ≈ 2.7 nm, as shown in Figure 2d,g. This value is consistent with the molecular length of C12-Ph-BTBT (it was estimated to be 27.1 Å by materials studio software), and suggests that C12-Ph-BTBT is preferentially oriented upright on the Si substrate. In order to access the SmX phase, we annealed the as-deposited sample at 140 °C for 10 min (Figure 1b). As seen in Figure 2b,e, this thermal treatment results in a polycrystalline thin film with very large domains whose sizes are between 2 and 20 μm with a median size of around 8 μm , as shown in Figure S3 (Supporting Information). Furthermore, the step height increases from ≈ 2.7 to ≈ 5.4 nm with annealing, as seen in Figure 2h. This observation suggests a bilayer structure formation, and is consistent with the transition from a unilamellar to bilayer structure seen in Ph-BTBT-10 polycrystalline thin film upon annealing reported by Iino et al.^[17] In order to obtain the SmE phase, we annealed the as-deposited sample at 170 °C for 5 min (Figure 1b). As seen in Figure 2c,f, we can see larger domains with a step height of ≈ 5.4 nm (Figure 2i). However, the polycrystalline thin film dewets into isolated droplets after annealing at this temperature.

We conducted GIXD experiments in order to elucidate the morphologies of C12-Ph-BTBT thin films in different smectic phases. Figure 3a–c shows 2D-GIXD patterns of C12-Ph-BTBT thin films as-deposited, annealed at 140 °C and annealed at 170 °C. Figure 3d shows the out-of-plane X-ray diffraction traces of these samples at $q_{xy} = 0 \text{ \AA}^{-1}$ extracted from their 2D-GIXD patterns. After annealing the samples, we observe reflections with an out-of-plane periodicity of 0.105 \AA^{-1} as opposed to out-of-plane periodicity of 0.210 \AA^{-1} that is seen in the GIXD pattern of the as-deposited film. Consistent with the AFM measurements, this change indicates an increase in the out-of-plane dimension by two times compared with that in the as-deposited film, which can be attributed to a transition from a unilamellar structure to bilayer structure.^[17] As opposed to Ph-BTBT-10, our C12-Ph-BTBT thin films retain their bilayer structure even after annealing at 170 °C indicating improved thermal stability of the bilayer structure. Although as seen in Figure 2c, the polycrystalline thin film appears to dewet into isolated droplets after annealing the films at 170 °C, the periodic reflections that are retained in the XRD pattern (Figure 3d and Figure S4 (Supporting Information)) suggests that the polycrystalline thin films reconstruct from the SmE phase upon cooling. Using a home-written software^[23] and using the monoclinic crystal

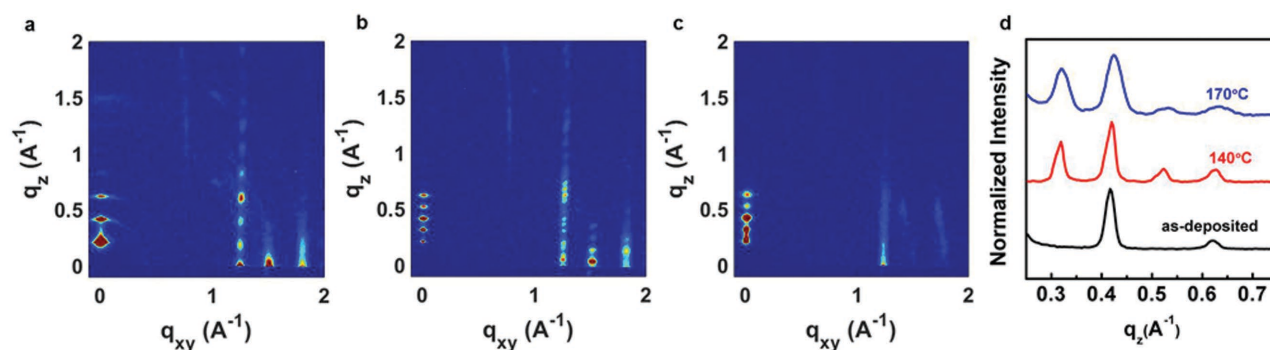


Figure 3. 2D-GIXD pattern of C12-Ph-BTBT thin films a) as-deposited, b) annealed at 140 °C, and c) annealed at 170 °C. d) Out-of-plane X-ray diffraction trace at $q_{xy} = 0 \text{ \AA}^{-1}$ extracted from the 2D-GIXD patterns of C12-Ph-BTBT thin films before and after annealing at 140 and 170 °C.

structure reported for Ph-BTBT-C10 as a starting point,^[24] we obtained a unit cell for the as-deposited sample and for the sample annealed at 140 °C that matches the reflections in their GIXD patterns. We find the as-deposited C12-Ph-BTBT thin films to adopt an orthorhombic crystal structure with the Pma2 space group having lattice dimensions $a = 6.26 \text{ \AA}$, $b = 8.24 \text{ \AA}$, $c = 29.8 \text{ \AA}$, $\alpha = \gamma = \beta = 90^\circ$ (Figure S5a, Supporting Information). We find C12-Ph-BTBT thin films that are annealed at 140 °C to instead adopt a monoclinic structure with P21/c space group having lattice dimensions $a = 59.6 \text{ \AA}$, $b = 8.24 \text{ \AA}$, $c = 6.26 \text{ \AA}$, $\alpha = \gamma = 90^\circ$, and $\beta = 104^\circ$ (Figure S5b, Supporting Information). Although the out-of-plane reflections of the samples annealed at 140 and 170 °C thin films are identical at $q_{xy} = 0 \text{ \AA}^{-1}$, we observe additional reflections along $q_{xy} = 1.42 \text{ \AA}^{-1}$ in the X-ray diffraction pattern of the sample that is annealed at 170 °C that do not

appear in the GIXD pattern of the sample annealed at 140 °C. This change indicates a decrease in space-group symmetry and suggests a polymorphic transformation that is consistent with our speculation of a transition between SmX and SmE phases. However, due to a lack of distinct reflections in the GIXD pattern of the sample annealed at 170 °C, we are not able to determine the lattice parameters that match its GIXD pattern.

Unlike in the case of Ph-BTBT-10, for C12-Ph-BTBT, the polycrystalline thin films that are obtained after annealing at the temperatures of both the SmX and the SmE phase exhibit the bilayer structure. We speculate that the bilayer structure comprises of two BTBT cores facing each other in the SmX phase; these adjacent cores represent an extended pi-conjugated system effectively.

Figure 4 shows the OTFT fabrication procedure and the polarized optical microscope images of the channels of these

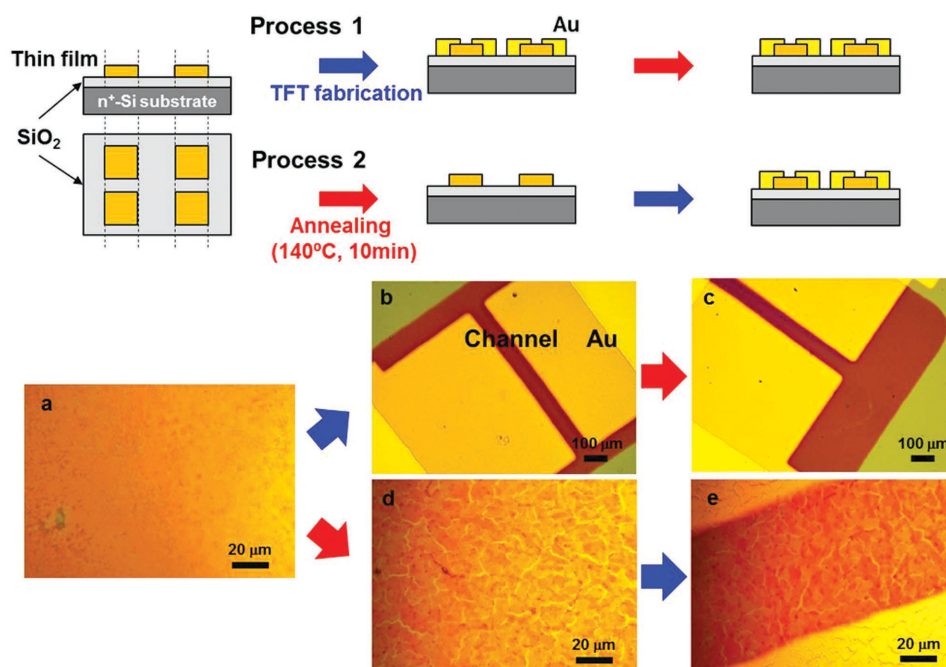


Figure 4. OTFT-fabrication procedures. The fabricated OTFTs have the top contact and bottom gate configuration. Process 1: Deposited electrodes on the as-deposited films, and then annealed the devices. Process 2: Annealed C12-Ph-BTBT films before depositing the electrodes. The polarized microscope images of C12-Ph-BTBT thin film a) as-deposited, b) after depositing the Au electrodes, and c) after the devices are annealed at 140 °C. The polarized microscope images of C12-Ph-BTBT thin film d) after annealing at 140 °C, and e) after depositing the Au electrodes.

devices. After depositing C12-Ph-BTBT thin films (≈ 50 nm) on the octyltrichlorosilane (OTS) modified SiO_2 (250 nm)/ n^+ -Si substrates, we fabricated OTFTs with the top-contact and bottom-gate configuration by two methods. In one case, we deposited electrodes on the as-deposited films, and then annealed the devices (Process 1). In the second case, we annealed C12-Ph-BTBT films before depositing the electrodes (Process 2). Gold (Au) was used as source and drain electrodes with a thickness of ≈ 50 nm, and annealing was performed at 140°C for 10 min in a glove box. A comparison of Figure 4c with Figure 4e reveals that larger domains are formed when the devices are prepared through Process 2 instead of Process 1. The difference in the domains sizes could be due to the presence of Au electrodes retarding the phase transition of C12-Ph-BTBT thin films. In order to clarify, we removed the Au electrodes from the annealed OTFTs by etching with aqua regia, and the detailed method is shown in Figure S6 (Supporting Information). Figure S6a (Supporting Information) shows the POM image of the annealed device. Figure S6b,d (Supporting Information) shows the POM images, and Figure S6f,h (Supporting Information) shows the AFM images of the exposed areas (areas that were not covered by the Au electrodes) and the areas that were originally covered by the Au electrodes during annealing, respectively, after the devices are immersed into aqua regia. The POM and AFM images obtained after etching of the gold electrodes from the device that is annealed at 140°C show that the grain size in the exposed areas increases in comparison to the as-deposited case; whereas the grain size stays the same in the areas that were covered by the Au electrode during annealing. Based on the AFM images, the exposed areas have step heights of 5.4 nm which indicates C12-Ph-BTBT adopts a bilayer structure in the exposed areas after annealing. In addition, when the films are further annealed after the removal of the Au electrodes, the grain sizes in both the exposed and the originally Au covered areas increase. The above phenomena indicate that the Au electrodes may be restricting surface diffusion of the molecules in the lateral direction to limit the formation of large grains.

In order to investigate the field-effect properties of OTFTs based on C12-Ph-BTBT, devices were fabricated by vacuum-deposition on OTS treated Si/SiO₂ substrates at room temperature. C12-Ph-BTBT's phase behavior on the OTFT performance is studied by annealing the OTFTs at different temperatures based on the phase transition temperatures found by DSC (Figure 1b and Figure S7a (Supporting Information)). Figure 5 and Figure S8 (Supporting Information) show transfer curves ($I_{\text{DS}}-V_{\text{G}}$ characteristics) and output curves ($I_{\text{D}}-V_{\text{DS}}$ characteristics) of these devices. Figure S8a,d (Supporting Information) shows the performance of devices without annealing (as-deposited). Figure S8b,e (Supporting Information) shows the electrical characteristics of devices fabricated through Process 1 (postannealed), and Figure 5c,f shows the electrical characteristics of the devices fabricated through Process 2 (preannealed). As can be

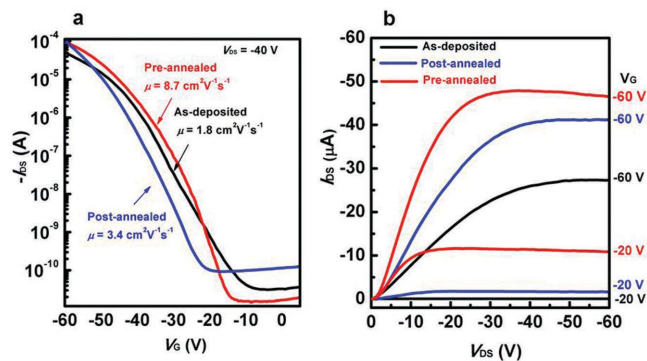


Figure 5. C12-Ph-BTBT-based OTFT characteristics: a) transfer curve ($I_{\text{DS}}-V_{\text{G}}$ characteristics) and b) output curve ($I_{\text{D}}-V_{\text{DS}}$ characteristics) of as-deposited (without annealing), postannealed (the OTFTs were fabricated first, and then annealed at 140°C), and preannealed (the OTFTs fabricated after the thin films were annealed at 140°C) devices, respectively.

seen, the OTFT transfer characteristics strongly depend on the annealing temperatures and the device fabrication process. The results of C12-Ph-BTBT-based OTFT performance are summarized in Table 1. As seen in Table 1, all devices show typical p-channel FET responses. The OTFTs without annealing exhibit a maximum mobility of $2.0\text{ cm}^2\text{ V}^{-1}\text{ s}^{-1}$ with an average mobility of $1.7 \pm 0.2\text{ cm}^2\text{ V}^{-1}\text{ s}^{-1}$. On the other hand, the OTFTs fabricated by Process 1 and annealed at 100°C exhibits a higher mobility of up to $2.3 \pm 0.3\text{ cm}^2\text{ V}^{-1}\text{ s}^{-1}$ with an on-off ratio of 3.7×10^6 . The OTFT performance further improves, yielding an average mobility of $3.4 \pm 0.4\text{ cm}^2\text{ V}^{-1}\text{ s}^{-1}$ and a maximum mobility of $4.0\text{ cm}^2\text{ V}^{-1}\text{ s}^{-1}$ after thermally annealing at 140°C . In addition, the device performance is maintained at temperature of 160°C , as shown in Figure S9 (Supporting Information), indicating the better thermal stability of C12-Ph-BTBT based OTFTs in comparison to Ph-BTBT-C10 based OTFTs reported.^[17] However, the OTFT mobility decreases to $0.46 \pm 0.29\text{ cm}^2\text{ V}^{-1}\text{ s}^{-1}$ after the devices are thermally annealed at 170°C (SmE phase) for 5 min due to dewetting of the thin films (Figure 2c,f). To confirm the air stability of the OTFTs based on C12-Ph-BTBT, the mobility values in ambient air operation were investigated by comparing the $I_{\text{D}}-V_{\text{G}}$ curves in

Table 1. OTFT performance of C12-Ph-BTBT-based devices.

	T^{c} [$^\circ\text{C}$]	$\mu_{\text{sat}}^{\text{d}}$ [$\text{cm}^2\text{ V}^{-1}\text{ s}^{-1}$]	$I_{\text{on}}/I_{\text{off}}$	V_{th} [V]	S [V per decade]
Process 1 ^a)	25	1.7 ± 0.2 (2.0) ^c)	$(1.0 \pm 0.6) \times 10^6$	-41.2 ± 2.6	8.2 ± 0.8
	100	2.3 ± 0.3 (2.8)	$(3.7 \pm 1.8) \times 10^6$	-44.5 ± 1.6	7.8 ± 0.3
	140	3.4 ± 0.4 (4.0)	$(3.1 \pm 6.1) \times 10^7$	-38.1 ± 4.3	7.2 ± 1.9
	170	0.46 ± 0.30 (1.2)	$(4.0 \pm 6.7) \times 10^6$	-41.5 ± 3.5	6.9 ± 1.8
Process 2 ^b)	100	2.8 ± 0.4 (3.4)	$(1.9 \pm 2.7) \times 10^7$	-42.5 ± 1.7	7.4 ± 1.1
	140	8.0 ± 0.3 (8.7)	$(1.1 \pm 0.4) \times 10^6$	-45.2 ± 1.4	7.6 ± 0.30
	170		No test		

^a) The devices were thermally annealed at various temperatures after the Au electrode deposition; ^b) The thin-films (vacuum-deposition) were thermally annealed before the OTFT fabrication; ^c) Annealing temperatures; ^d) All the data were reported in average value from more than eight devices. The values in parenthesis represent the maximum mobility.

the same device stored and operated in ambient air. The performances of OTFTs based on C12-Ph-BTBT were not significantly degraded after storage in ambient air for ten months (Figure S11, Supporting Information).

Interestingly, the device performance is enhanced when the OTFTs are fabricated by Process 2. The average mobility of C12-Ph-BTBT-based OTFT is dramatically increased to $8.0 \pm 0.3 \text{ cm}^2 \text{ V}^{-1} \text{ s}^{-1}$, with the best device reaching to a mobility of $8.7 \text{ cm}^2 \text{ V}^{-1} \text{ s}^{-1}$. This result is higher than the devices which are annealed at the same temperature after depositing the Au electrodes (fabricated by Process 1). We observe similar enhancements in mobility when the sample is annealed at $100 \text{ }^\circ\text{C}$ for 10 min (Figure S10, Supporting Information), although the domain size is smaller (less than $8 \mu\text{m}$ as shown in Figure S12 (Supporting Information)). The above results indicate that the highly ordered liquid crystalline phase of C12-Ph-BTBT is conducive to charge transport. The high threshold voltages exist in all the devices. This may be due to the highest occupied molecular orbital (HOMO) level of C12-Ph-BTBT (-5.64 eV) not matching well with the work function of gold (5.2 eV), and the charge trap states limiting the charge injection. A higher mobility can be achieved by choosing a different electrode in the OTFT fabrication.

3. Conclusions

In summary, we have successfully synthesized an air-stable and high charge-carrier mobility calamitic liquid-crystalline molecule, C12-Ph-BTBT, that exhibits a highly ordered SmX ($X = \text{K}$ or H) liquid-crystalline phase. The C12-Ph-BTBT based OTFTs have mobilities as high as $4.0 \text{ cm}^2 \text{ V}^{-1} \text{ s}^{-1}$ after thermal annealing the devices at $140 \text{ }^\circ\text{C}$ (SmX phase). Most interestingly, the mobility of OTFTs dramatically increases to $8.7 \text{ cm}^2 \text{ V}^{-1} \text{ s}^{-1}$ if C12-Ph-BTBT thin films are thermally annealed at $140 \text{ }^\circ\text{C}$ before the S/D electrodes deposition. Our results also show that the polycrystalline thin films that are obtained after annealing the films at the SmX and the SmE phases exhibit a bilayer structure, and the highest charge-carrier mobility is observed in the OTFTs based on the polycrystalline films that are obtained from the solid-like highly ordered SmX phase. We conclude that C12-Ph-BTBT can be used to fabricate polycrystalline thin films with high uniformity for OTFTs, showing the potential of this compound for future applications in organic electronics.

4. Experimental Section

Materials: The C12-Ph-BTBT were prepared by the palladium-catalyzed Suzuki–Miyaura coupling reaction between 2-bromo[1]benzothieno[3,2-*b*]benzothiophene and 2-(4-dodecylphenyl)-4,4,5,5-tetramethyl-1,3,2-dioxaborolane as indicated in the Supporting Information. The chemical structure of C12-Ph-BTBT was confirmed by NMR and HRMS. The liquid crystal properties of this material were examined by DSC, POM, and XRD.

Morphological Analysis of C12-Ph-BTBT Thin Films: C12-Ph-BTBT was evaporated on an OTS-modified Si/SiO₂ substrate under vacuum to form uniform thin films. The films were annealed at various temperatures (100 , 140 , and $170 \text{ }^\circ\text{C}$, respectively) for the AFM, POM, and XRD studies to compare the morphology of the annealed films with the as-deposited

films. GIXD experiments were conducted at the G1 station ($11.2 \pm 0.05 \text{ keV}$) of the Cornell High Energy Synchrotron Source. The beam was chosen to be 0.05 mm tall and 1 mm wide. The width of each sample was 5 mm . The X-ray beam was aligned above the critical angle of C12-Ph-BTBT thin film but below that of the substrate, at a 0.17° incident angle with the substrate. X-ray scattering was collected with a 2D CCD detector, positioned 119.4 mm from the sample. All GIXD images had been background subtracted.

OTFT Fabrication and Characterization: OTFT devices were fabricated in a top-contact, bottom-gate configuration on a highly doped n-type Si wafers with 250-nm thick thermally grown SiO₂ grown by dry thermal oxidation served for substrates and gate electrode. The wafers were modified with OTS according to the ref. [25]. The organic semiconductor layers were prepared via vacuum-deposition (50 nm) on the treated substrates at room temperature. Gold films (50 nm) as drain and source electrodes were deposited through a metal shadow mask on to as-deposited thin films or on to thin films that were annealed at 100 or $140 \text{ }^\circ\text{C}$. The drain–source channel width (W)/length (L) were $380/38$, $580/58$, $780/78$, and $980/98 \mu\text{m}$, respectively. After the deposition of Au electrodes on the as-deposited films, the OTFT devices were annealed at 100 , 140 , or $170 \text{ }^\circ\text{C}$. The characteristics of the OTFT devices were measured in ambient conditions using a Keithly 4200 and Agilent B500 semiconductor parameter analyzer. By employing the following formula, the field-effect mobility (μ_{FTT}) was extracted from the saturation regime ($V_d = -40 \text{ V}$) of the I_d by employing the following formula

$$I_d = (W/2L)\mu_{\text{FTT}}C_i(V_g - V_{\text{th}})^2 \quad (1)$$

where I_d was the drain current, C_i indicated the capacitance per unit area of the SiO₂ modified with OTS insulator, and V_g and V_{th} represented the gate and threshold voltages, respectively. The current on/off ($I_{\text{on}}/I_{\text{off}}$) ratio was determined from the current I_d at $V_g = -60 \text{ V}$ and $V_g = 0 \text{ V}$.

Supporting Information

Supporting Information is available from the Wiley Online Library or from the author.

Acknowledgements

This work was financially supported by Shenzhen Science and Technology Research Grant (ZDSYS20140509094114164), Nanshan Innovation Agency Grant (KC2015ZDYF0016A), Guangdong Key Research Project (2014B090914003 and 2015B090914002), Guangdong Talents Project, NSFC (51373075), National Basic Research Program of China (973 Program, No. 2015CB856500), Guangdong Academician Workstation (2013B090400016) Natural Science Foundation of Guangdong Province (2014A030313800) and China Postdoctoral Science Foundation (2015M570892). Portion of this work was conducted at the Cornell High Energy Synchrotron Source (CHESS), which was supported by the National Science Foundation and the National Institutes of Health/National Institute of General Medical Sciences under NSF award DMR-1332208.

Received: May 2, 2016

Revised: June 21, 2016

Published online:

- [1] J. H. Cho, J. Lee, Y. Xia, B.-S. Kim, Y. He, M. J. Renn, T. P. Lodge, C. D. Frisbie, *Nat. Mater.* **2008**, *7*, 900.
- [2] I. Yagi, N. Hirai, Y. Miyamoto, M. Noda, A. Imaoka, N. Yoneya, K. Nomoto, J. Kasahara, A. Yumoto, T. Urabe, *J. Soc. Inf. Disp.* **2008**, *16*, 15.

- [3] K. Myny, S. Steudel, S. Smout, P. Vicca, F. Furthner, B. van der Putten, A. K. Tripathi, G. H. Gelinck, J. Genoe, W. Dehaene, P. Heremans, *Org. Electron.* **2010**, *11*, 1176.
- [4] T. Sekitani, U. Zschieschang, H. Klauk, T. Someya, *Nat. Mater.* **2010**, *9*, 1015.
- [5] M. Noda, N. Kobayashi, M. Katsuhara, A. Yumoto, S. Ushikura, R. Yasuda, N. Hirai, G. Yukawa, I. Yagi, K. Nomoto, T. Urabe, *J. Soc. Inf. Disp.* **2011**, *19*, 316.
- [6] U. Zschieschang, M. J. Kang, K. Takimiya, T. Sekitani, T. Someya, T. W. Canzler, A. Werner, J. Blochwitz-Nimoth, H. Klauk, *J. Mater. Chem.* **2012**, *22*, 4273.
- [7] K. Nakayama, Y. Hirose, J. Soeda, M. Yoshizumi, T. Uemura, M. Uno, W. Li, M. J. Kang, M. Yamagishi, Y. Okada, E. Miyazaki, Y. Nakazawa, A. Nakao, K. Takimiya, J. Takeya, *Adv. Mater.* **2011**, *23*, 1626.
- [8] H. Minemawari, T. Yamada, H. Matsui, J. Tsutsumi, S. Haas, R. Chiba, R. Kumai, T. Hasegawa, *Nature* **2011**, *475*, 364.
- [9] O. Goto, S. Tomiya, Y. Murakami, A. Shinozaki, A. Toda, J. Kasahara, D. Hobar, *Adv. Mater.* **2012**, *24*, 1117.
- [10] G. Schweicher, V. Lemaire, C. Niebel, C. Ruzié, Y. Diao, O. Goto, W.-Y. Lee, Y. Kim, J.-B. Arlin, J. Karpinska, A. R. Kennedy, S. R. Parkin, Y. Olivier, S. C. Mannsfeld, J. Cornil, Y. H. Geerts, Z. Bao, *Adv. Mater.* **2015**, *19*, 3066.
- [11] Y. Yuan, G. Giri, A. L. Ayzner, A. P. Zoombelt, S. C. Mannsfeld, J. Chen, D. Nordlund, M. F. Toney, J. Huang, Z. Bao, *Nat. Commun.* **2014**, *5*, 3005.
- [12] N. Onojima, I. Shintani, S.-I. Kitahara, T. Takahashi, T. Kato, Y. Haramoto, *Phys. Status Solidi C* **2011**, *8*, 607.
- [13] A. J. van Breemen, P. T. Herwig, C. H. Chlon, J. Sweelssen, H. F. Schoo, S. Setayesh, W. M. Hardeman, C. A. Martin, D. M. de Leeuw, J. J. Valetton, C. W. Bastiaansen, D. J. Broer, A. R. Popa-Merticaru, S. C. Meskers, *J. Am. Chem. Soc.* **2006**, *128*, 2336.
- [14] E. Lim, Y. M. Kim, J.-I. Lee, B.-J. Jung, N. S. Cho, J. Lee, L.-M. Do, H.-K. Shim, *J. Polym. Sci., Part A: Polym. Chem.* **2006**, *44*, 4709.
- [15] H. Iino, J.-I. Hanna, *J. Appl. Phys.* **2011**, *109*, 074505.
- [16] H. Iino, J. Hanna, *Adv. Mater.* **2011**, *23*, 1748.
- [17] H. Iino, T. Usui, J. Hanna, *Nat. Commun.* **2015**, *6*, 6828.
- [18] A. Kim, K. S. Jang, J. Kim, J. C. Won, M. H. Yi, H. Kim, D. K. Yoon, T. J. Shin, M. H. Lee, J. W. Ka, Y. H. Kim, *Adv. Mater.* **2013**, *25*, 6219.
- [19] G. K. Dutta, S. Guha, S. Patil, *Org. Electron.* **2010**, *11*, 1.
- [20] J.-I. Hanna, A. Ohno, H. Iino, *Thin Solid Films* **2014**, *554*, 58.
- [21] J. Hanna, T. Kobori, T. Usui, Y. Takayashiki, H. Iino, A. Oono (PTC), *US Patent Application No. 14/003933*, 2012.
- [22] I. Dierking, *Texture of Liquid Crystals*, Wiley-VCH, Weinheim, Germany **2003**, Ch. 1.
- [23] A. K. Hailey, A. M. Hiszpanshi, D.-M. Smilgies, Y.-L. Loo, *J. Appl. Crystallogr.* **2014**, *47*, 2090.
- [24] S. Inoue, H. Minemawari, J. Y. Tsutsumi, M. Chikamatsu, T. Yamada, S. Horiuchi, M. Tanaka, R. Kumai, M. Yoneya, T. Hasegawa, *Chem. Mater.* **2015**, *27*, 3809.
- [25] H. Meng, F. Sun, M. B. Goldfinger, G. D. Jaycox, Z. Li, W. J. Marshall, G. S. Blackman, *J. Am. Chem. Soc.* **2005**, *127*, 2406.